

Electron spin relaxation and quantum localization in carbon nanoparticle: Electron spin echo studies

Stefan Lijewski,¹ Magdalena Wencka,¹ Stanislaw K. Hoffmann,^{1,*} Mateusz Kempinski,²
Wojciech Kempinski,¹ and Malgorzata Sliwinska-Bartkowiak²

¹*Institute of Molecular Physics, Polish Academy of Sciences, Smoluchowskiego 17, 60-179 Poznan, Poland*

²*Institute of Physics, Adam Mickiewicz University, Umultowska 85, 61-614 Poznan, Poland*

(Received 18 December 2006; revised manuscript received 7 September 2007; published 30 January 2008)

We present pulsed electron spin resonance measurements of activated carbon fibers (ACFs) for pristine samples and after adsorption of nitrobenzene in the fibers' porous structure. Two-level tunneling state (TLS) model is discussed in order to define the nature of paramagnetic centers and to explain the electron spin-lattice relaxation mechanism in the studied system. Electron spin echo decay is dominated by spin diffusion at low temperatures (below 7 K) and for higher temperatures the echo dephasing rate is governed by thermal excitations of the TLS model. The model enables us to treat the nanographitic units being the basic structural units of ACF, as quantum wells (dots) separated by potential barriers of the order of $25(2) \text{ cm}^{-1}$ determined from temperature dependence of the spin-lattice relaxation rate. Stimulation of these barriers leads to spin localization within nanographitic units. A possible control of the potential barriers is the crucial point for the problem of nanographitic unit system treated as a quantum dot matrix.

DOI: [10.1103/PhysRevB.77.014304](https://doi.org/10.1103/PhysRevB.77.014304)

PACS number(s): 73.20.-r, 73.22.-f, 74.78.Na, 76.30.-v

I. INTRODUCTION

Nanosized carbon systems having low-dimensional structures such as carbon nanotubes, graphene layers or ribbons, and activated carbon fibers are of current interest due to their unconventional properties¹ and potential applications in nanotechnology and nanoelectronics.² A single sheet of graphite called graphene has peculiar electronic and magnetic properties resulting from quantum size effect and can display semiconducting or semimetallic character.^{3,4} Thermally excited electrons in graphene behave like relativistic particles called massless Dirac fermions and travel at very high speed of 10^6 m/s . Thus they conduct electricity with virtually no resistance and move as if they were light waves.⁵ Fractional quantum Hall effect and Berry phase have been discovered in such materials.^{6,7}

The general problem in the above mentioned graphitic structures, including fullerenes,⁸ is that these materials are expected to be diamagnetic. However, the magnetic properties were discovered by magnetization measurements even in the pure graphitic states,^{9,10} and clearly evidenced by strong electron spin resonance (ESR) signals.¹¹⁻¹⁴ A specific source of the magnetism observed in experiments, i.e., an origin of unpaired spins in pure graphitic state and in graphitic structures, is still a subject of debate.^{9,15-19} In this paper we consider this problem in activated carbon fibers.

Activated carbon fibers (ACFs) consist of graphite nanoparticles and are activated by heat treatment with simultaneous creation of nanoporosity. ACFs are a three-dimensional disordered system of nanographitic units. Every unit (grain) is approximately of 2.5 nm in diameter, contains three to six graphene sheets, and has mass of about 10^{-19} g . The number of sheets can be evaluated from the shape of Raman bands.²⁰ The perfect *AB* stacking, existing in crystalline graphite, is disturbed in ACF nanoparticles.²¹ Moreover, a slip of graphene planes produces orientational disorder, i.e., platelet-to-platelet angle can be randomly and widely distrib-

uted. Interplane distance (0.353–0.378 nm) is greater than in pure graphite (0.335 nm) and the planes are not necessary equidistant. Another disorder can occur at nanographitic unit edges (peripheral disorder), which are a combination of the zigzag and armchair arrangements of the peripheral carbon atoms. The disorder manifests itself as defect-type bands (*D* bands) in Raman spectra.^{20,22} The edge shape and system size critically determine the electronic and magnetic properties of ACF. Nonbonding π -electron states (edge states) are created around the zigzag edges and can be the source of spin magnetism due to electron localization. The magnetism can be affected by various chemical species such as hydrogen and oxygen, which can terminate the peripheral carbon atoms.

The electric properties of an ACF sample are determined by intergrain contacts mainly and the conductivity is characteristic of granular conducting systems.²³ The size of slit-shaped pores, existing between nanographitic units, is approximately 1.2–1.4 nm. Thus ACF samples are highly porous with specific surface area up to $3000 \text{ m}^2/\text{g}$ and have typical density of 1.6 g/cm^3 . The large specific surface area and highly uniform porosity of ACF make them good and selective adsorbents used in environmental toxin and pesticide removal, protein separation, gas storage, and purification filtering of organic solvents or white wine.

Adsorption of oxygen, nitrogen, and helium gas affects the magnetic, electric, and structural properties of ACF.²⁴ Swelling of nanopores induced by gas uptake was observed. Adsorbed oxygen induces structural rearrangement and charge transfer from ACF to adsorbed oxygen. An influence of adsorbed hydrogen atoms on magnetic properties of carbon nanotubes was observed by ESR.²⁵ A liquid adsorbed in porous structure can also modify ACF properties. Moreover, this gives a possibility of observation of molecules confined in nanometer pores.²⁶ The effect of H_2O , CCl_4 , and $\text{C}_6\text{H}_5\text{NO}_2$ adsorption in ACF^{23,27} was studied, as an increase of potential barrier for charge carrier hopping and an increase in the spin localization.

The best method for studying magnetic properties and dynamics of radicals in carbon structures is ESR, which allows distinguishing between various types of the radicals and determination of the spin concentration. ESR signal of crystalline “bulk” graphite is characteristic of conduction electron spin resonance with the single line of the Dysonian shape.^{28–30} ESR signal of polycrystalline graphite also comes from the highly delocalized unpaired electrons (charge carriers).¹³ Similarly as for bulk graphite the ESR spectrum consists of a single asymmetrical Dysonian line, which becomes symmetrical and Lorentzian for highly dispersed graphite powders when microcrystal dimension becomes lower than the skin depth (few microns). This line is relatively narrow (0.3 mT) and homogeneously broadened due to motional narrowing effect produced by dynamical delocalization of the unpaired electrons over large number of grains. Conduction electron spin resonance was observed also in single-wall and multiwalled nanotubes but with broader Dysonian lines (1–2.5 mT).^{31,32} Two symmetrical Lorentzian lines were distinguished in ESR spectrum of nanohorns prepared by a laser evaporation of graphite.³³ The broad line (0.45 mT) sensitive for oxygen arises from amorphous interior of nanohorns whereas the narrow line (0.25 mT) is due to the charge carriers in two-dimensional graphenelike sheets.

ESR signals in nanographitic units of ACF display Lorentzian line shape since the nanoparticle dimensions are lower than the skin depth. Thus, the line shape cannot simply identify a conduction electron ESR signal. In nanographite prepared by heat treatment of diamond nanoparticles the two-component ESR spectrum was recorded.³⁴ Above 170 K the single broad signal with the linewidth growing with temperature (peak-to-peak linewidth=3.7 mT at 295 K) was observed and assigned to π electrons at the graphene edge states. At lower temperatures an additional narrow signal appears with the temperature independent linewidth 0.4–0.5 mT. This signal was assigned as due to localized spins associated with structural defects.

We recently published ESR studies of activated carbon fibers.^{23,35} We have shown that ESR spectrum of pristine ACF consists of a single narrow ($\Delta B_{pp}=0.32$ mT) Lorentzian line at $g=2.0031$. The ESR signal is assigned as due to localized unpaired electrons (not to the charge carriers) and its linewidth is temperature independent. When H_2O , CCl_4 , and $C_6H_5NO_2$ molecules were adsorbed in ACF then a three-component ESR spectrum was observed. Except for the narrow line characteristic of pristine ACF two broader Lorentzian lines appear. The second signal ($\Delta B_{pp}\approx 2$ mT) was assigned to host nanographitic units surrounded by guest molecules captured into ACF nanopores. The broadest component shows strong increase of the linewidth with temperature from 4.5 mT at 10 K to 13 mT at 120 K. This line was assigned to the surface centers of ACF.

In this paper we describe the results of pulsed ESR measurements, both of pure ACF and of ACF with adsorbed guest nitrobenzene molecules ($NB=C_6H_5NO_2$), which deliver information on nature and dynamics of paramagnetic centers in nanographitic systems and on the host-guest interaction. The host-guest interactions determine the possibilities

of spin manipulations in ACF treated as a quantum dots matrix.²³ Spin population control is very important from the point of view of possible future spintronic applications of nanographitic unit system.³⁶

Pulsed electron spin resonance methods use electron spin echo (ESE) signal for studying dynamical behavior of a spin system by observation of spin system magnetization behavior after short (nanoseconds) microwave pulse excitation. Pulsed ESR has not been applied so far for investigation of nanographitic systems, although it offers very promising possibilities. In contrast to classical continuous wave ESR, which operates on resolved spectral lines, the ESE methods work on much narrower nonresolved spin packets forming inhomogeneously broadened ESR lines. Electron spin echo can be excited for inhomogeneously broadened ESR lines only. This allows immediate distinguishing between ESR signals of delocalized spins (conduction electrons) having homogeneously broadened ESR lines and ESR signals of localized spins.

A spin packet is a group of spins having the same resonance Larmor frequency. Spin packets forming an ESR line differ slightly in this frequency and are a consequence of nonresolved superhyperfine structures or inhomogeneity of the system or the external magnetic field. Because the spin packets are very narrow (typically tens of microtesla), they are very sensitive to molecular and atomic dynamics. ESE signal allows observation of fast relaxation processes in unpaired electron spin systems. Magnetization of a spin system disturbed by pulse excitation returns to the equilibrium in time order of seconds at liquid helium temperature and microseconds at room temperature. It is due to spin-lattice relaxation processes. Moreover, microwave pulses of resonance frequency produce coherent precession motion of electron magnetic moments of spin packets. Dephasing of the coherent precession appears in time of nano- to microseconds and is visible as electron spin echo signal decay. The decay rate is sensitive to spin diffusion and spectral diffusion within the spin system and to local motions of a radical center or its surrounding.

Spin-lattice relaxation has been considered with relation to the broad ESR line (2 mT at 4.2 K) in graphite nanoparticles prepared by heating of diamond nanoparticles.³⁴ The relaxation time $T_1\approx 10$ ns was estimated from the linewidth of the homogeneously broadened ESR line at room temperature and the relaxation was described in terms of scattering processes of conduction electrons related to the π -electron edge states. In this paper we present relaxation of electron spins localized in ACF structure.

II. EXPERIMENT

ACF samples were acquired from Osaka Gas Chemicals Co. Ltd., Japan. The ACF samples with pore size 1.2–1.4 nm were used. Before adsorption of the nitrobenzene guest, the ACF samples were evacuated at 200 °C at 10^{-4} mbar for 1 h to ensure that the pores are empty. The nitrobenzene underwent triple distillation process in order to remove water and oxygen impurities. The samples for ESR measurements were degassed and sealed under vacuum to avoid contact with atmospheric oxygen.

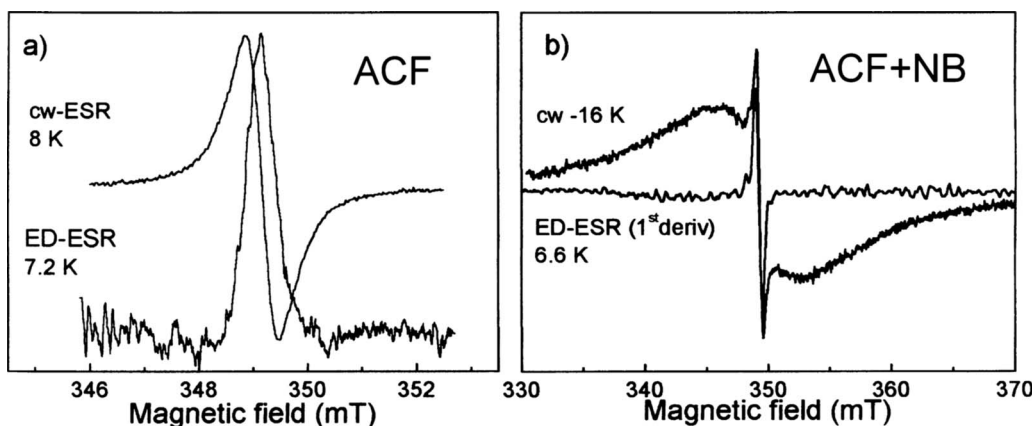


FIG. 1. cw-ESR and ED-ESR spectra at low temperatures: (a) pristine ACF. The ED-ESR signal is recorded in the form of absorption curve, whereas cw-ESR signal is recorded as the first derivative of the absorption. (b) In the cw-ESR spectrum of ACF+NB the three components can be distinguished (Refs. 23 and 35), whereas in ESE experiments the echo signal can be induced with spins in narrowest line only. The ED-ESR line is differentiated for better comparison with cw-ESR spectrum.

ESE measurements were performed with a Bruker ESP 380E FT/CW spectrometer equipped with an Oxford CF935 flow helium cryostat. Two types of pulsed experiments were performed. At first we recorded electron spin resonance spectrum using pulse excited electron spin echo signal (echo detected ESR=ED-ESR). In the second experiment we measured the electron spin-lattice relaxation using saturation recovery method and the electron phase relaxation (ESE dephasing) by ESE decay. The measurements were performed in the temperature range 5–38 K. At higher temperatures the ESE signal vanishes in the spectrometer dead time (about 80 ns) due to the very fast ESE dephasing and simultaneously the electric conductivity becomes too high even for continuous wave ESR spectrum detection.

In the ED-ESR experiment the two-pulse ESE amplitude is registered when external magnetic field is swept through the ESR spectrum. The ED-ESR spectrum has the absorption shape and allows differentiating between lines having different ESE dephasing time called the phase memory time T_M . The two-pulse sequence used in this experiment was the same as used during spin-lattice relaxation time measurements described below. The spin-lattice relaxation time T_1 was determined by measurements of the ESE amplitude after pulsed saturation with the pulse of 72 ns duration for pure ACF and 56 ns for ACF+NB sample. The full saturation was achieved with these pulses. The recovery of the magnetization was observed using a Hahn-type ESE signal generated by two identical 48 ns pulses with the interpulse interval 200 ns for the pure ACF sample and 80 ns-200 ns-48 ns sequence for ACF+NB sample. The pulse duration was experimentally chosen to obtain full saturation and maximal echo amplitude. The recovery of the magnetization after saturation was described as a sum of two exponential functions in the whole temperature range. The shorter component is weaker and is temperature independent. This component becomes negligible at higher temperatures and it seems to be an artifact, so we present results for T_1 time derived from the longer exponential recovery component.

The phase memory time T_M , describing the dephasing of the spin precession motion (ESE amplitude decay), was mea-

sured with the same two-pulse sequence as used during the spin-lattice relaxation measurements. The echo signal decay was exponential over the whole temperature range.

III. RESULTS AND DISCUSSION

A. Electron spin echo detected electron spin resonance spectrum

Low temperature ESR spectrum of ACF recorded as the first derivative of the absorption (typical continuous wave ESR spectrum) and the pure absorption spectrum recorded by the ED-ESE method are compared in Fig. 1(a). The single ESR line of 0.32 mT linewidth is well reproduced by the ED-ESR line. The existence of the ESE signal in the pristine ACF is a proof that ESR line is inhomogeneously broadened. This confirms that the unpaired spins are localized in the nanographitic particles. Two questions should be answered: (1) What is the reason of the inhomogeneous broadening, i.e., what is an origin of spin packets forming the ESR line? Two possibilities can be considered. ESR g factors can be slightly different for radical centers located in different sites of the sample. Such dispersion of g value is generally observed in disordered and amorphous solids and has been observed in coal samples also.³⁷ It seems that small g -factor dispersion can take place in nanographitic units of ACF. The second possibility is related to dangling bonds on peripheries of pure nanographitic units. These bonds are practically saturated and it can be due, at least partially, by attaching hydrogen atoms during ACF preparation. Hyperfine coupling between unpaired electron spins and hydrogen nuclei will produce inhomogeneous broadening of ESR line. The latter possibility can be rather excluded, as it will be seen from the results of ESE dephasing experiments. (2) More fundamental question is related to the origin of unpaired spin states in ACF. There is still not definite answer for this question. Five different structure defects have been so far considered as responsible for unpaired electron creation: (a) dangling σ bonds on edges of graphene sheets;¹⁶ (b) a defect in a form of adatom, which can be a carbon atom lying on a graphene

plane and bridging a carbon-carbon bond on the graphene surface; (c) a carbon vacancy formed by removing a carbon atom from graphene sheet and relaxing to the pentagon structure;¹⁷ (d) sterically protected carbon radicals which are immobilized in the aromatic system of sp^2 bonded carbons;¹⁸ and (e) localized nonbonding π -electron states at zigzag graphene edges.^{9,20,33}

It should be noted that the density of the unpaired spins is very low. It is known that there exists one unpaired electron per 60 carbon atoms in graphite and per over 10^4 atoms in carbon nanotubes.³² In graphite nanoparticles formed from diamond nanoparticles by heating, the rather high density $10^{19}/\text{g}$ of the unpaired spins was found.³⁴ We evaluated this density in our ACF samples, from ESR line intensity at 40 K with respect to ultramarine standard, as being $3.6 \times 10^{14}/\text{g}$. This is relatively low density indicating that in ACF there is about 3.6×10^{-5} unpaired spins per nanographitic unit (assuming single nanographitic unit mass $\approx 10^{-19}$ g). Low density of the radical centers and its uncontrolled dependence on a graphitic system and preparation method indicate that the unpaired electrons are localized onto structural defects and rather are not related to the nondisturbed structure of graphene sheets forming the nanographitic particles.

After treatment of the ACF with nitrobenzene the ESR spectrum essentially changes [Fig. 1(b)]. Except the narrow (0.32 mT) line the two additional broader components appear in the spectrum. The 1.9 mT broad line is temperature independent and corresponds to $6.3 \times 10^{15}/\text{g}$ spin density. The broadest line with the peak-to-peak width 4.0 mT at 4.2 K corresponds to the spin density $1.3 \times 10^{17}/\text{g}$. This line broadens with heating. Electron spin echo detected ESR spectrum [shown as its first derivative in Fig. 1(b)] clearly displays signal from the narrowest line only, the same as in pristine ACF, except a small increase in the line amplitude. Thus, the two spectral lines are homogeneously broadened and are due to unpaired spins delocalized over nanographitic units.

It seems that the two broadest lines can correspond to the ESR lines observed in the graphite nanoparticles created from diamond nanoparticles.³⁴ Thus, the similar paramagnetic defects can be created by liquids adsorbed in nanopores of graphitic nanoparticles and by graphitization of nanodiamond powder at high temperatures (above 1500 °C) in an inert atmosphere. This suggests that the delocalized spins appear on grain surfaces.

B. Electron spin-lattice relaxation

Spin-lattice relaxation rate $1/T_1$ is typical for amorphous systems where phonon-type dynamics does not exist, i.e., the relaxation rate $1/T_1$ is relatively fast at very low temperatures (as compared to crystalline solids) and rather slowly grows with temperature. Temperature dependence of the relaxation rate in pristine ACF and after nitrobenzene adsorption is presented on Fig. 2. The dependence is well described by the following equation:

$$\frac{1}{T_1} = aT + b \operatorname{cosech}\left(\frac{\Delta}{kT}\right) \quad (1)$$

with parameters $b = 3.9 \times 10^5 \text{ s}^{-1}$, $\Delta = 24(2) \text{ cm}^{-1} = 35 \text{ K} = 0.28 \text{ kJ/mol}$. The linear term aT appears only in the

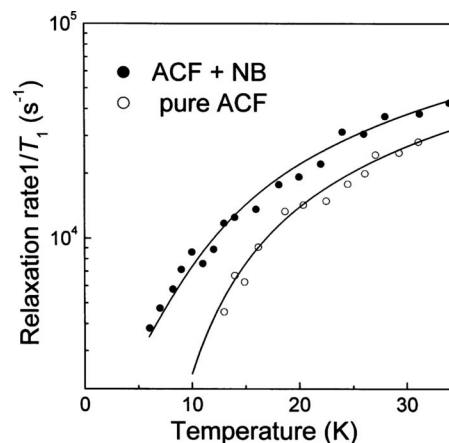


FIG. 2. Temperature dependence of the spin-lattice relaxation rate $1/T_1$ for ACF and ACF+NB samples. The solid lines are the best fits to Eq. (1) with thermally activated process having activation energy 24 cm^{-1} .

nitrobenzene treated samples ACF+NB with $a = 550 \text{ s}^{-1} \text{ K}^{-1}$. This term generally appears in samples where distribution of paramagnetic centers is not perfectly uniform.³⁸ The second term describes the relaxation mechanism operating in nanographitic units. Relaxation theories predict that this mechanism can be related to (a) two-level tunneling states (TLSs);^{39–41} (b) local tunneling oscillators having large amplitude of vibration and trapped in a symmetrical double potential well having two low-lying vibrational states with splitting Δ and not populated excited vibrational states. The experimental Δ value seems to be too small for this mechanism (typically $\Delta = 80–150 \text{ cm}^{-1}$);⁴² (c) Murphy mechanism⁴² which involves spin diffusion and phonon-induced simultaneous spin flip and an excitation of a local vibrational state of surrounding molecules such as reorienting NH_3 groups and mediated by spin-spin dipole coupling.⁴³ This mechanism can be excluded in nanographitic units, except the case when tunneling molecular groups are attached to peripheral dangling bonds; (d) relaxation via a small number of rapidly relaxing pairs of paramagnetic centers in the case when pair-bath relaxation is the rate-limiting step in the overall relaxation process.⁴⁴ Radical pair formation is practically not probable for such small overall spin densities as we determined in our samples. Moreover the ESR spectra do not show any trace of pair lines.

Thus the most probable mechanism of the electron spin-lattice relaxation in nanographitic structure are thermal excitations between TLSs having splitting $\Delta = 24 \text{ cm}^{-1}$. TLS is a theoretical concept, which assumes that the potential energy surface of an amorphous or disordered solid contains many shallow asymmetric local minima, which can be approximated by a collection of two-level double wells. In disordered and amorphous materials such potential minima can be imagined as two local conformations of molecules or two possible sites for some atoms. Possible orientational and peripheral disorders in nanographitic units, described in the Introduction, can lead to the TLSs. Also tunneling of a carbon adatom between two positions can produce spin relaxation described in terms of TLS theory. We are not able to identify

the molecular origin of the TLSs in the studied material. The electron spin-lattice relaxation mechanism involves coupling of a radical center to the phonon-induced relaxation of a nearby-localized TLS.⁴⁰ The energy Δ in Eq. (1) should be treated as an average energy difference between ground states of various TLSs, which are expected to have a dispersion of Δ values due to a disorder existing in a solid. The dispersion of Δ in ACF is very small, similarly to very small dispersion in g factors, otherwise the recovery of magnetization would be described not by the pure exponential function $M_z = M_0[1 - \exp(-t/T_1)]$ but by stretched exponential $M_z = M_0[1 - \exp(-t/T_1)^\beta]$ with stretched exponent β related to the degree of the disorder as generally observed in amorphous materials.⁴⁵ The very small dispersion of Δ and g factor indicates that the studied ACF is a very homogeneous system with a very small dispersion between nanographitic units. It suggests that TLSs are intrinsic property of the nanograins which is detected by paramagnetic centers. The TLS-containing nanographitic particles of AFCs can be considered as quantum wells or quantum dots,⁴⁶ as we already mentioned discussing electric conductivity results.²³ They have spins localized within nanoparticles and well defined discrete energy levels without distribution of parameters. Thus, except for well known quantum dots in semiconducting nanocrystals which confine electric charge carrier motions in all spatial directions,⁴⁶ we suggest their existence in graphitic nanoparticles. One should notice, that the quantum dot concept is not restricted to semiconducting and metallic⁴⁷ nanocrystals, and that our idea of quantum dots, localized in graphitic nanoparticles, well inscribes in general picture of low-dimensional nanosized quantum system. All atoms are quantum dots. Quantum dots were identified in micelles of biological systems,⁴⁸ in molecular metal redox centers,⁴⁹ and in living cells and dyes.⁵⁰ Quantum dots are called qubits in quantum computing nanotechnology, and the “quantum dot-cellular automata” is a promising concept in molecular electronics.⁵¹

C. Electron spin echo dephasing (phase relaxation)

After pulsed excitation the electron spin echo signal quickly decays. Various processes producing randomization of the precession phase of excited spins can produce the decay. As the result the perpendicular magnetization, formed by a coherent precession of spins excited by the first pulse, decays in time and vanishes in typical time of microseconds. The two-pulse ESE amplitude V decay is characterized by so-called phase memory time T_M , which in a simple case of exponential decay, is defined by the equation $V(\tau) = V_0 \exp(-2\tau/T_M)$ where τ is the interpulse interval. The decay of ESE amplitude in ACF and ACF+NB is shown in Fig. 3. The decay rate is different in both samples and does not show any electron spin echo decay envelope modulation, which is generally produced by weak dipolar interactions with surrounding magnetic nuclei. It means that in pristine ACF the edge dangling bonds are not saturated with protons and that after nitrobenzene adsorption there is no interaction between localized spins and nitrobenzene protons and/or nitro-nuclei. This indicates that the radical centers, local-

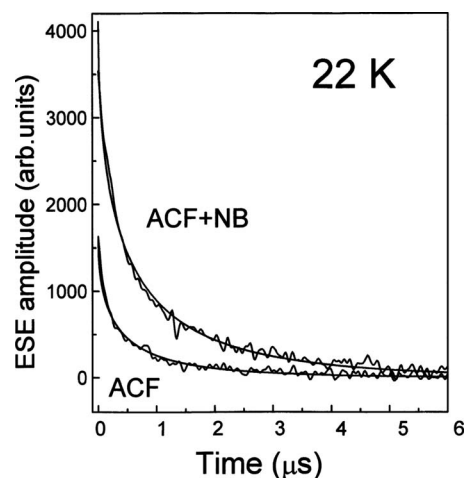


FIG. 3. Electron spin echo amplitude decay in ACF and ACF+NB at 22 K. The recovery is exponential and shown by the solid lines resulting from Eq. (2).

ized in pristine ACF structure and giving narrowest ESR line, are located at a distance larger than about 0.5 nm from nanopores where nitrobenzene molecules are adsorbed. The ESE decay was exponential in the whole temperature range and described by the equation

$$V(\tau) = V_0 \exp(-a\sqrt{\tau} - b\tau). \quad (2)$$

The best fit to Eq. (2) is shown by solid lines in Fig. 3.

The first term in Eq. (2) is characteristic of spin diffusion, i.e., a transfer of spin excitation energy between excited and nonexcited spins of the system.^{43,52} This is due to dipole-dipole flip-flops and thus is temperature independent. The second term in Eq. (2), i.e., $V_0 \exp(-b\tau)$, can have a few sources:⁵² (a) instantaneous diffusion,⁵³ i.e., dephasing produced by the second microwave pulse which perturbs dipolar coupling between excited spins (the instantaneous diffusion is temperature independent); (b) molecular motions which produce temperature dependent broadening of the spin packets forming an ESR line;⁵⁴ (c) spin-lattice relaxation processes effective in higher temperature range.⁵⁴ It should be noted that for samples with adsorbed nitrobenzene, where microwave pulses excite only spins in the narrowest inhomogeneously broadened line, the spin diffusion and instantaneous diffusion are governed by dipolar coupling within the whole spin system, i.e., spins in both nonexcited lines are also involved.

Figure 3 shows that the phase relaxation is faster in pristine ACF samples than in ACF with adsorbed nitrobenzene. It suggests that adsorbed molecules influence the ESE dephasing mechanism. A difference in behavior of pure ACF and ACF+NB is well visible in temperature dependence of the phase memory T_M . The effective phase memory time T_M characterizing total decay described by Eq. (2) is defined as the time where ESE amplitude V decreases to V_0/e value. The temperature dependence of the dephasing rate $1/T_M$ is shown in Fig. 4. This experimental dependence is well described by the following equation:^{54,55}

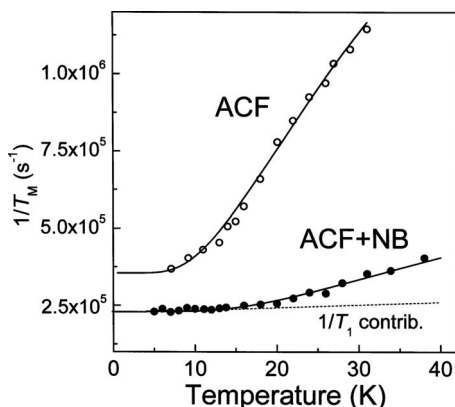


FIG. 4. Temperature dependence of the ESE dephasing rate $1/T_M$ (T_M is the phase memory time). The exponential increase in $1/T_M$ is due to thermally activated motion with activation energy 27 cm^{-1} for ACF and 44 cm^{-1} for ACF+NB.

$$\frac{1}{T_M} = \left(\frac{1}{T_M} \right)_0 + \left(\frac{1}{T_1} \right) + c \exp\left(-\frac{\Delta E}{kT} \right), \quad (3)$$

where c is a coupling coefficient.

The temperature independent term $(1/T_M)_0$ is due to spin diffusion and instantaneous diffusion and has a different value in ACF and in ACF+NB. The lowering of the $(1/T_M)_0$, when NB is adsorbed in ACF, is due to a screening of the paramagnetic centers by nitrobenzene molecules leading to a decrease in effective dipolar coupling between unpaired electrons. The second term describes possible ESE dephasing due to spin-lattice relaxation processes. The contribution of this term is temperature dependent as visible in Fig. 3 and is simply calculated using the parameters of Eq. (1). This contribution is very small and is shown by a dashed line in Fig. 4. The exponential term in Eq. (3) is related to molecular dynamics in a slow motion range⁵² and is responsible for the temperature dependence of the dephasing rate. The best fit of Eq. (3) to the experimental points is shown by a solid line in Fig. 4 with parameters listed in Table I. An increase in $1/T_M$ with temperature indicates that the spin packet width ΔB_{packet} grows with temperature as a result of molecular motions in which the radical center is involved. The ΔB_{packet} is related to the dephasing rate as

$$\frac{1}{T_M(s)} = \frac{\sqrt{3} g \mu_B}{2 h} \Delta B_{\text{packet}}(T), \quad (4)$$

which gives $\Delta B_{\text{packet}} = 9 \mu\text{T}$ at 10 K both for ACF and ACF+NB, and $\Delta B_{\text{packet}} = 26 \mu\text{T}$ for ACF at 25 K. These very narrow spin packets are easily influenced by molecular dynamics.⁴⁵

The above results show that molecular motions in nanographitic units are strongly suppressed when adsorbed NB is frozen in nanopores at low temperatures. It is reflected by an increase in activation energy ΔE and a decrease in the coupling coefficient c in Eq. (3). The value of $\Delta E = 27 \text{ cm}^{-1}$ determined from the phase relaxation is, within experimental accuracy, the same as value $\Delta E = 24 \text{ cm}^{-1}$ determined from temperature dependence of the spin-lattice relaxation. It means that the same thermally activated motion (TLS dynamics) is a source of both the spin-lattice relaxation and the ESE dephasing, although mechanisms of the relaxations are different.

IV. CONCLUSIONS

Activated carbon fibers show granular structure and display electronic conductivity limited by tunneling or hopping of charge carriers between grains with activation energy 219 cm^{-1} for hopping.²³ At low temperatures (below 100 K) the itinerant electrons become progressively localized allowing observation of ESR signal^{23,35} and generation of ESE signal below 40 K. The low temperature localization of unpaired electrons is evidenced in electron spin echo experiments. An ESE signal can be induced only when the ESR line is inhomogeneously broadened, which is not possible for dynamically delocalized centers. The line inhomogeneity seems to result from dispersion of the ESR g factors. The dispersion is relatively small indicating a good homogeneity of the granular system.

Electron spin relaxation delivers information about internal dynamics of nanographitic units. Both the spin-lattice relaxation and phase relaxation data indicate that this dynamics can be described as thermal excitations in double well potential with average activation energy of about $25(2) \text{ cm}^{-1}$ (average from T_1 and T_M results), which can be described in terms of the TLS model. This model shows that individual nanographitic unit can be treated as a quantum well (dot) having localized spin states. To find mobile electrons out of the edge, a potential barrier stimulation between separated nanographitic units is necessary.

When nitrobenzene molecules are adsorbed in nanopores of the ACF, the two broad lines appear additionally in the ESR spectrum. The spins of these lines do not produce ESE signal, thus are homogeneously broadened due to unpaired electron delocalization. Guest nitrobenzene molecules reduce the spin diffusion and/or instantaneous diffusion, which are governed by dipole-dipole coupling between unpaired electrons. Nitrobenzene influences also the TLS dynamics producing an increase in the barrier height between potential wells from 25 to 44 cm^{-1} . The results suggest that one can

TABLE I. Parameters used for best fit of Eq. (3) to experimental points in Fig. 4.

	$(1/T_M)_0$	c	ΔE
ACF	$3.7 \times 10^5 \text{ s}^{-1}$	$3.48 \times 10^6 \text{ s}^{-1}$	$27(2) \text{ cm}^{-1} = 0.32 \text{ kJ/mol}$
ACF+NB	$2.3 \times 10^5 \text{ s}^{-1}$	$8.5 \times 10^6 \text{ s}^{-1}$	$44(8) \text{ cm}^{-1} = 0.52 \text{ kJ/mol}$

influence the potential barrier between TLS states in ACF particles both by the temperature and by guest molecules adsorbed in porous system of ACF. This can be related to a reduction in size of nanographitic unit produced by guest molecules^{35,56} and/or changes in the edge states present around the peripheries of the graphene sheets,³⁴ which are in contact with guest molecules located in nanopores. Finally, we conclude that both the results for pristine ACF and for ACF with adsorbed guest molecules indicate possibilities of

control of nanographitic unit system treated as a quantum dot matrix.

ACKNOWLEDGMENTS

This work was partially supported by the Grant MNiI No. N202 058 31/3121 and by the grant within the framework of the 2.6 ZPORR "Regional Innovation Strategy and Knowledge Transfer" program, cofinanced by the European Social Fund and Polish State Treasury.

*skh@ifmpan.poznan.pl

- ¹M. S. Dresselhaus, G. Dresselhaus, and P. C. Eklund, *Science of Fullerenes and Carbon Nanotubes* (Academic, San Diego, CA, 1996).
- ²M. S. Dresselhaus, G. Dresselhaus, and P. Avouris, *Topics in Applied Physics* (Springer, Heidelberg, 2001), Vol. 80.
- ³S. Saito, M. S. Dresselhaus, and G. Dresselhaus, *Physical Properties of Carbon Nanotubes* (Imperial College, London, 1998).
- ⁴J. C. Meyer, A. K. Geim, M. I. Katsnelson, K. S. Novoselov, T. J. Booth, and S. Roth, *Nature* (London) **446**, 60 (2007).
- ⁵K. S. Novoselov, A. K. Geim, S. V. Morozov, D. Jiang, M. I. Katsnelson, I. V. Grigorieva, S. V. Dubons, and A. A. Firsov, *Nature* (London) **438**, 197 (2005).
- ⁶J. Alicea and M. P. A. Fisher, *Phys. Rev. B* **74**, 075422 (2006).
- ⁷Y. Zhang, Y. Tan, H. L. Stormer, and P. Kim, *Nature* (London) **438**, 201 (2005).
- ⁸J. Stankowski, L. Piekara-Sady, W. Kempinski, O. Huminiacki, and P. B. Sczaniecki, *Fullerene Sci. Technol.* **5**, 1203 (1997).
- ⁹Y. Shibayama, H. Sato, T. Enoki, and M. Endo, *Phys. Rev. Lett.* **84**, 1744 (2000).
- ¹⁰T. Makarova, *Semiconductors* **38**, 615 (2004).
- ¹¹W. Kempinski, P. Scharff, J. Stankowski, L. Piekara-Sady, and Z. Trybua, *Physica C* **274**, 232 (1997).
- ¹²A. I. Shames, A. M. Panich, W. Kempinski, A. E. Alexenskii, M. V. Baidakova, A. T. Dideikin, V. Y. Osipov, V. I. Siklitski, E. Osawa, and M. Ozawa, *J. Phys. Chem. Solids* **63**, 1993 (2002).
- ¹³L. S. Singer and G. Wagoner, *J. Chem. Phys.* **37**, 1812 (1962).
- ¹⁴K. Sugihara, *J. Phys. Soc. Jpn.* **53**, 393 (1984).
- ¹⁵K. Wakabayashi, M. Sigrist, and M. Fujita, *J. Phys. Soc. Jpn.* **67**, 2089 (1998).
- ¹⁶V. Barone, O. Hod, and G. E. Scuseria, *Nano Lett.* **6**, 2794 (2006).
- ¹⁷Y. Ma, P. O. Lehtinen, A. S. Foster, and R. M. Nieminen, *New J. Phys.* **6**, 68 (2004).
- ¹⁸N. Park, M. Yoon, S. Berber, J. Ihm, E. Osawa, and D. Tomanek, *Phys. Rev. Lett.* **91**, 237204 (2003).
- ¹⁹K. Nakada, M. Fujita, G. Dresselhaus, and M. S. Dresselhaus, *Phys. Rev. B* **54**, 17954 (1996).
- ²⁰M. A. Pimenta, G. Dresselhaus, M. S. Dresselhaus, L. G. Cancado, A. Jorio, and R. Saito, *Phys. Chem. Chem. Phys.* **9**, 1276 (2007).
- ²¹Y. Kobayashi, K. Takai, K. I. Fukui, T. Enoki, K. Harigaya, Y. Kaburagi, and Y. Hishiyama, *Phys. Rev. B* **69**, 035418 (2004).
- ²²A. Rao, A. Fung, M. Dresselhaus, and M. Endo, *J. Mater. Res.* **7**, 1788 (1992).
- ²³M. Kempinski, W. Kempinski, J. Kaszynski, and M. Sliwinska-Bartkowiak, *Appl. Phys. Lett.* **88**, 143103 (2006).
- ²⁴N. Kobayashi, T. Enoki, C. Ishii, K. Kaneko, and M. Endo, *J. Chem. Phys.* **109**, 1983 (1998).
- ²⁵K. Shen, D. L. Tierney, and T. Peitrass, *Phys. Rev. B* **68**, 165418 (2003).
- ²⁶R. Radhakrishnan, K. E. Gubbins, and M. Sliwinska-Bartkowiak, *Phys. Rev. Lett.* **89**, 076101 (2002).
- ²⁷M. Kempinski, W. Kempinski, and M. Sliwinska-Bartkowiak, *Rev. Adv. Mater. Sci.* **11**, 34 (2006).
- ²⁸G. Wagoner, *Phys. Rev.* **118**, 647 (1960).
- ²⁹M. S. Dresselhaus and G. Dresselhaus, *Adv. Phys.* **30**, 139 (1981).
- ³⁰S. Chehab, K. Guerin, J. Amiel, and S. Flandrois, *Eur. Phys. J. B* **13**, 235 (2000).
- ³¹P. Petit, E. Jouguelet, J. E. Fischer, A. G. Rinzler, and R. E. Smalley, *Phys. Rev. B* **56**, 9275 (1997).
- ³²F. Beuneu, C. l'Huillier, J. P. Salvetat, J. M. Bonard, and L. Forro, *Phys. Rev. B* **59**, 5945 (1999).
- ³³S. Garaj, L. Thien-Nga, R. Gaal, L. Forro, K. Takahashi, F. Kokai, M. Yudasaka, and S. Iijima, *Phys. Rev. B* **62**, 17115 (2000).
- ³⁴O. E. Andersson, B. L. V. Prasad, H. Sato, T. Enoki, Y. Hishiyama, Y. Kaburagi, M. Yoshikawa, and S. Bandow, *Phys. Rev. B* **58**, 16387 (1998).
- ³⁵M. Kempinski, W. Kempinski, and M. Sliwinska-Bartkowiak, *Acta Phys. Pol. A* **108**, 339 (2005).
- ³⁶M. Kempinski, M. Sliwinska-Bartkowiak, and W. Kempinski, *Rev. Adv. Mater. Sci.* **14**, 14 (2007).
- ³⁷A. Y. Bresgunov, O. G. Poluektov, Y. Lebedev, A. L. Barra, L. C. Brunel, and J. Roberts, *Chem. Phys. Lett.* **175**, 624 (1990).
- ³⁸S. Hoffmann, W. Hilezer, J. Goslar, and M. Augustyniak-Jablokow, *J. Phys.: Condens. Matter* **13**, 7443 (2001).
- ³⁹W. A. Phillips, *J. Low Temp. Phys.* **7**, 351 (1972).
- ⁴⁰S. R. Kurtz and H. J. Stapleton, *Phys. Rev. B* **22**, 2195 (1980).
- ⁴¹S. K. Hoffmann, W. Hilezer, and T. Radczyk, *Acta Phys. Pol. A* **103**, 373 (2003).
- ⁴²J. Murphy, *Phys. Rev.* **145**, 241 (1966).
- ⁴³T. Ichikawa and V. V. Kurshev, *J. Chem. Phys.* **99**, 5728 (1993).
- ⁴⁴M. B. Schultz and C. D. Jeffries, *Phys. Rev.* **149**, 270 (1966).
- ⁴⁵S. K. Hoffmann, W. Hilezer, J. Goslar, S. Kiczka, and I. Polus, *Phys. Chem. Chem. Phys.* **4**, 4944 (2002).
- ⁴⁶E. Borovitskaya and M. Shur, *Quantum Dots. Selected Topics in Electronics and Systems* (World Scientific, Singapore, 2002), Vol. 25.
- ⁴⁷J. Buttet, R. Car, and C. W. Myles, *Phys. Rev. B* **26**, 2414 (1982).

- ⁴⁸B. Dubertret, P. Skouris, D. Norris, V. Noiveaux, A. Bivanlou, and A. Libchaber, *Science* **298**, 1759 (2002).
- ⁴⁹B. Xu and N. Tao, *Science* **301**, 1221 (2003).
- ⁵⁰W. Funnel and D. Magsinger, *J. Nanobiotechnology* **4**, 10 (2006).
- ⁵¹C. Lent, B. Isaksen, and M. Lieberman, *J. Am. Chem. Soc.* **125**, 1056 (2003).
- ⁵²K. M. Salikhov and Y. D. Tsvetkov, *Time Domain Electron Spin Resonance* (Wiley, New York, 1979), Chap. 7, pp. 231–278.
- ⁵³V. V. Kurchev and T. Ichikawa, *J. Magn. Reson.* (1969-1992) **96**, 563 (1992).
- ⁵⁴S. K. Hoffmann, J. Goslar, W. Hilczer, M. A. Augustyniak-Jablokov, and S. Kiczka, *J. Magn. Reson.* **153**, 56 (2001).
- ⁵⁵S. Kiczka, S. Hoffmann, J. Goslar, and L. Szczepanska, *Phys. Chem. Chem. Phys.* **6**, 64 (2004).
- ⁵⁶H. Sato, N. Kawatsu, T. Enoki, M. Endo, R. Kobori, S. Maruyama, and K. Kaneko, *Solid State Commun.* **125**, 641 (2003).